 DOI: 10.1002/masy.200850501 

# Micro-Raman and Tip-Enhanced Raman Spectroscopy of Carbon Allotropes

*Günter G. Hoffmann,*[*1,2] *Gijsbertus de With,*[1] *Joachim Loos*[*1,3]

**Summary:** Raman spectroscopic data are obtained on various carbon allotropes like diamond, amorphous carbon, graphite, graphene and single wall carbon nanotubes by micro-Raman spectroscopy, tip-enhanced Raman spectroscopy and tip-enhanced Raman spectroscopy imaging, and the potentials of these techniques for advanced analysis of carbon structures are discussed. Depending on the local organisation of carbon the characteristic Raman bands can be found at different wavenumber positions, and e.g. quality or dimensions of structures of the samples quantitatively can be calculated. In particular tip-enhanced Raman spectroscopy allows the investigation of individual single wall carbon nanotubes and graphene sheets and imaging of e.g. local defects with nanometer lateral resolution. Raman spectra of all carbon allotropes are presented and discussed.

**Keywords:** carbon allotropes; graphene; raman spectroscopy; single wall carbon nanotubes; TERS

## Introduction

Carbon is known to exist in a number of allotropes, which range from the hardest of all known material, the pure and single crystalline diamond, to the soft, mainly amorphous, and very impure carbon in the form of soot or glassy carbon. Three of those, diamond, graphite, and of course soot are known since ancient times, while the monomolecular forms of carbon, carbon nanotubes and the Buckminsterfullerenes have been discovered only some years ago.[1,2] These forms can be classified as three-dimensional (diamond and graphite, Figure 1a and b), one-dimensional (single wall carbon nanotubes, Figure 1d), and zero-dimensional (Buckminsterfullerene, $C_{60}$, Figure 1e). Only recently, in 2004, Gaim and Novoselov[3] produced the two-dimensional form of carbon, graphene by ''simply'' removing sheet after sheet from graphite to gain a single graphene layer (Figure 1c); and attention is paid to this form of carbon because of its extraordinary functional properties, and potential low production costs.[4]

Since it is possible to produce the allotropes of carbon in large quantities, making it feasible to use them for numerous applications,[5] it has become more and more important to analyze these materials being able to establish, ultimately, structure-property relations at the nanometer length scale. Raman spectroscopy, and in particular micro-Raman,[6] surface enhanced Raman spectroscopy (SERS)[7] or tip-enhanced Raman spectroscopy (TERS) recently introduced[8,9] are characterisation techniques that are able to provide chemical as well as functional information on these materials.

The latter one, TERS, is a characterisation technique combining the power of Raman spectroscopy to reveal chemical composition and molecular structure with the ultra-high spatial resolution of scanning probe microscopy (SPM). Theoretically, TERS allows spectroscopic analysis of any kind of macromolecular material (as

[1] Eindhoven University of Technology, P.O. Box 513, 5600 MB Eindhoven, The Netherlands
E-mail: g.g.hoffmann@tue.nl
[2] University of Duisburg-Essen, Schützenbahn 70, D-45117 Essen, Germany
[3] Dutch Polymer Institute, P.O. Box 902, 5600 AX Eindhoven, The Netherlands
E-mail: j.loos@tue.nl

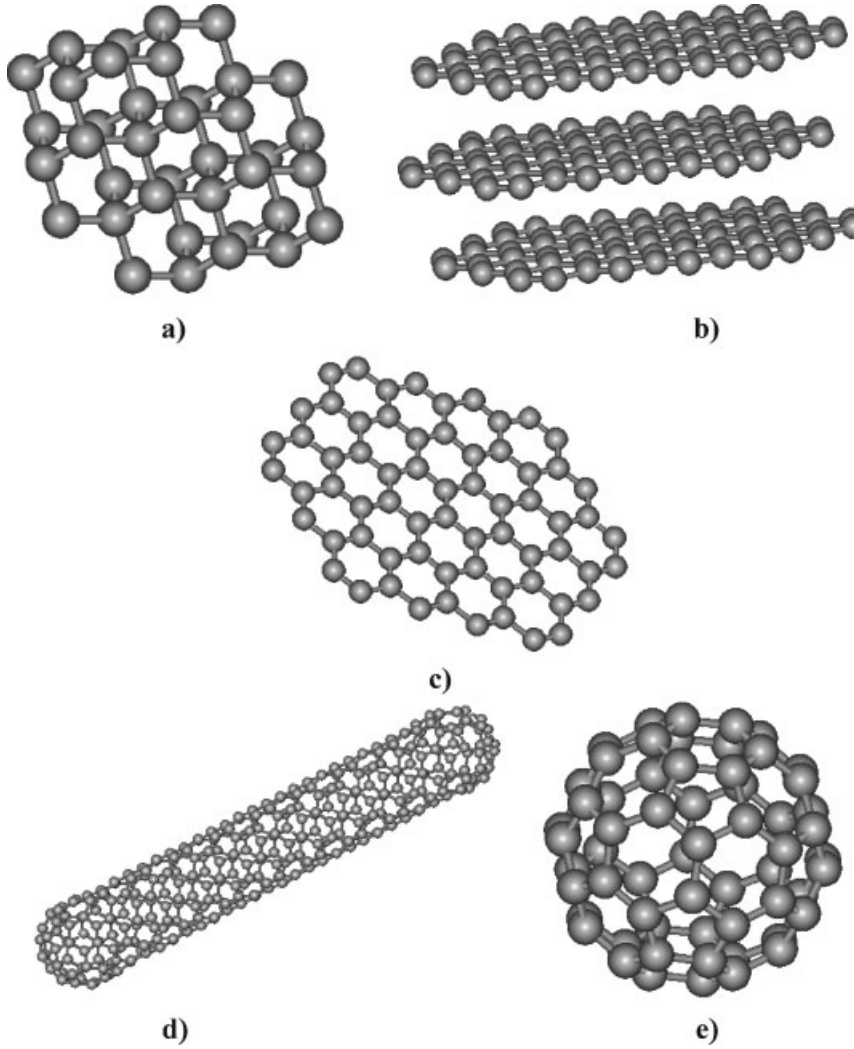


***Figure 1.***
(a) Diamond lattice and (b) graphite, both three-dimensional structures, (c) graphene (two-dimensional), d) single wall carbon nanotube (one-dimensional), and (e) Buckminsterfullerene (zero-dimensional).

well as inorganic materials like Si) with nanometer resolution, merely depending on probe quality. Only recently TERS imaging was demonstrated with lateral resolution far better than 50 nm and made it possible to identify local defects along one individual single wall carbon nanotube. The group of Novotny and Hartschuh[9–13] realized a resolution of 15 nm while reaching an enhancement of 4, whereas our group resolved about 30 nm while enhancing the $G^+$-line 256 times.[14]

The potential of TERS is enormous: TERS on biological macromolecules such as proteins and ribonucleic acid (RNA) as well as on various organic dyes has been demonstrated and resulted in spectra that are enhanced compared to conventional confocal Raman spectroscopy by factors $10^6$ to $10^{14}$, as claimed by the authors; on the other hand, from theoretical considerations even sub-nanometer spatial resolution, resolution below the curvature size of the actual SPM tip, should be possible to be

 

realised by tuning the interaction between tip and sample.

It is the purpose of our study to introduce recent results obtained on various carbon allotropes by micro-Raman spectroscopy and TERS. Main focus is to demonstrate that all carbon allotropes show variations in their Raman characteristics, which allows us, ultimately, to locally identify lateral variations of the composition or defects in carbon-based materials with nanometer resolution by means of TERS.

## Experimental Part

A general view of the multi-purpose scanning near-field optical spectrometer NTEGRA SPECTRA$^{TM}$ (NT-MDT) is shown in Figure 2. This back-scattered geometry based configuration for analysing a specimen on transparent substrates allows us to record: atomic force or shear force microscopy (AFM/SFM) images (topography, phase contrast, etc.), confocal optical images, confocal far-field Raman and fluorescence spectra and images, tip-enhanced near-field Raman spectra and images (fluorescence enhancement/quenching). A cw linearly-polarized laser beam from a He-Ne laser operating at 632.8 nm ($E = 1.96$ eV, $TEM_{00}$) enters the spectrometer through a single-mode optical fibre. The laser output passing through the plasma line filter is expanded and converted to a mode with a given polarization (linear, circular, radial, azimuthal). After that it is reflected by the edge-filter and goes into the inverted optical microscope (Olympus IX70) through an unpolarised beam-splitter cube (10/90) and a pinhole. A 100x oil immersion objective

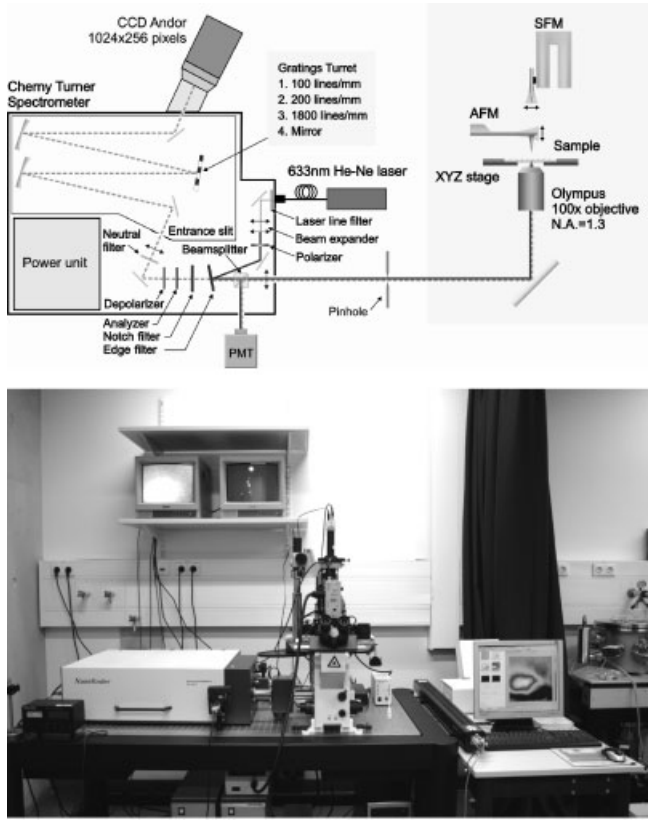


***Figure 2.***
(top) Optical setup of the TERS instrument used, and (bottom) photography of the TERS setup.

 

(Olympus, n.a.=1.3, refractive index of oil $n = 1.516$) focuses the laser beam into a spot with a size of less than 300 nm and the power at sample is about 100 μW. The tip is positioned into one of two longitudinal lobes near rims of the diffraction-limited laser spot to locally enhance the electromagnetic field beneath its apex. This system allows one to lock the tip position inside the laser spot to maintain optimum illumination conditions. A near-field Raman image is established by raster scanning the sample with a *xy*-scan stage equipped with a close-loop operation system. Scattered and/or reflected light is collected with the same objective and directed back to the spectrometer through the pinhole. An additional Kaiser notch-filter is installed into the optical path to suppress the Rayleigh scattering. In the laser confocal and spectral modes the light transmitted by the beam-splitter cube is detected with a photomultiplier (Hamamatsu, PMT943-02) and a thermoelectrically cooled charge-coupled detector (ANDOR, DV420), respectively. All Raman spectra were recorded within a spectral range of 150–2500 $cm^{-1}$. A 200 lines/mm grating provides a spectral resolution of better than 15 $cm^{-1}$. The pinhole size was equal to 40 μm because of making use of the 100x oil immersion objective.

### Sample Preparation

We utilized purified single wall carbon nanotubes (SWCNTs, HiPCo, Carbon Nanotechnology Inc.) as a proper one-dimensional object with strong Raman active spectral lines for testing ultrahigh spatial resolution. A dispersion was prepared by mixing 0.05 g SWCNTs with 20 g dichloromethane in a flask and then sonicating the resulting dispersion for about 1 hour. The sonication was carried out using a horn sonicator (Sonic Vibracell VC750) with a cylindrical tip (10 mm end cap in diameter). The output power was 20 W and, therefore, delivering energy was 1100–1200 J/min. The flask was placed inside a bath with ice water during sonication in order to prevent rising of the temperature. A droplet of this dispersion was spin coated at 300 rpm for 2 min on a microscopy cover glass slide. The glass slide was preliminarily cleaned in a ''piranha'' solution ($H_2SO_4$:$H_2O_2$) at ambient conditions for 30 min, then rinsed in $CH_3OH$ and finally dried under a continuous $N_2$-gas flow. A similar procedure was applied for preparation of graphene sheets but starting from highly oriented pyrolytic graphite (HOPG, NT-MDT), and for the $C_{60}$ material (Aldrich).

Transmission electron microscopy (TEM) investigation of graphene after dispersing in aqueous solutions were performed using a Tecnai 20 (FEI Co.) operated at 200 kV. The samples were prepared by dipping a copper TEM grid in the graphene dispersion and subsequent drying.

## Results and Discussion

### Diamond and Amorphous Carbon

The Raman spectrum of diamond has been reported to consist of a single sharp line at 1332 $cm^{-1}$ (e.g. Knight and White[15] and Figure 3). On the other hand, glassy carbon is a material composed of varying amounts of graphite and amorphous carbon. Two broad lines are observed at 1340 and 1590 $cm^{-1}$. These results are consistent with the turbostratic structure, which has been suggested for glassy carbon (with a particle size $L_a$ of approximately 30 Å) by Nathan *et al.*[16] The corresponding spectrum is shown in Figure 3. Diamond layers deposited by vapour deposition (CVD) find a growing number of applications e.g. in electronics technology due to their hardness, insulating properties and thermal conductivity while being transparent to broad ranges of UV, visible and infrared radiation.[5] In these layers small diamond crystallites are surrounded by graphite and amorphous carbon in the grain boundaries. Raman spectroscopy e.g. is applied to easily discriminate these non-diamondoid impurities by their variations of the Raman spectrum, and thus it is employed to judge the quality of such coatings.

 

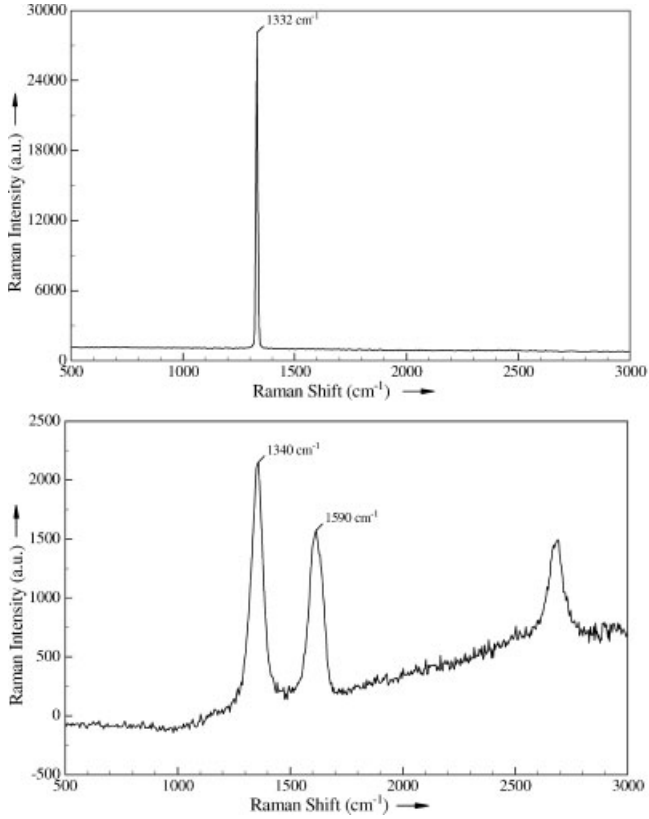


***Figure 3.***
(top) Micro-Raman spectroscopy spectra of a gem-quality (*tw, vsi*) diamond, and (bottom) glassy carbon.

**Graphite**

Another example on how Raman spectroscopy can distinguish between crystalline and amorphous order of carbon is presented by analyzing graphite. In single crystalline graphite Tuinstra and Koenig[17] only found a single line at 1575 $cm^{-1}$ (Figure 4). This is called the G-peak (from graphite). Analysing highly ordered pyrolytic graphite (HOPG) by micro-Raman spectroscopy we can confirm the presence of this band and only this band, which suggests that the sample has very high crystallinity. In graphite of lower quality, however, one also encounters a Raman band at 1355 $cm^{-1}$, called D-line (from disordered graphite, Figure 4b). The ratio G-band versus D-band Raman intensity tells us about the ordered/disordered state of graphite, and thus e.g. about its conductivity.

**$C_{60}$ Buckminsterfullerene**

Looking with Raman spectroscopy to Buckminsterfullerenes ($C_{60}$ molecules), on the other hand, results in more complex Raman spectra than for diamond, amorphous carbon or graphite. $C_{60}$ molecules are produced together with $C_{70}$ according to the method of Krätschmer *et al.*[18] by heating graphite in an inert gas. From the soot produced the pure compound can be separated by liquid chromatography on silica. Due to the high symmetry of the molecule, the infrared spectrum shows only four lines. The Raman spectrum, as it is complementary to the IR spectrum, shows much more lines, and if, measured with excitation by visible light, is complicated by the fact that a resonance Raman spectrum is produced. Bethune *et al.*[19] measured the Raman spectrum of $C_{60}$ with an argon ion laser and reported a line at 1470 $cm^{-1}$ as the strongest,

 

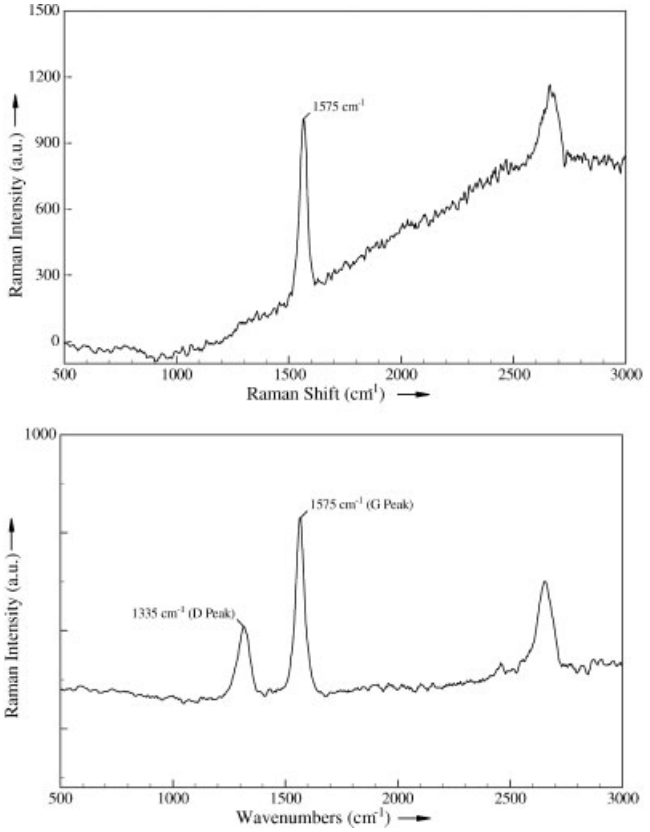


***Figure 4.***
Micro-Raman spectra of (top) highly ordered pyrolytic graphite, and (bottom) conventional graphite.

which corresponds well with our own measurements (Figure 5). Neugebauer *et al.*[20] calculated the Raman and IR vibrational spectrum of Buckminsterfullerenes on a high theoretical level, but without taking into account resonance effects. The visible lines in our experimental spectrum match the calculated ones in frequency but not in intensity, as

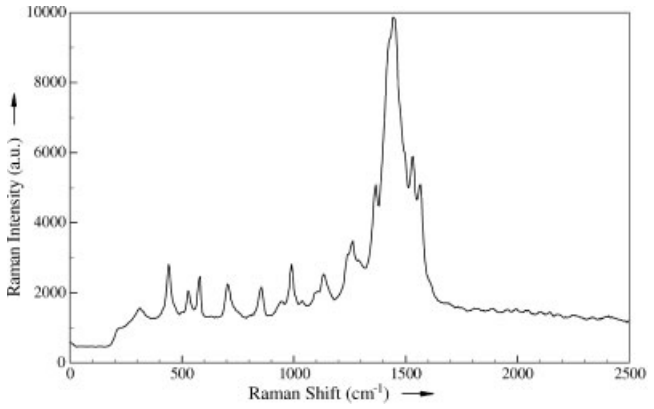


***Figure 5.***
Micro-Raman spectrum of a Buckminsterfullerene ($C_{60}$) film obtained with a laser source with wavelength of 633 nm.

 

our tip-enhanced Raman spectrum actually is a resonance Raman spectrum.

**Single Wall Carbon Nanotubes**

Single wall carbon nanotubes (SWCNTs) can be grown from the vapour phase at higher temperatures using transition metal catalysts. Formally one can build these tubes by rolling a single graphene sheet and connecting the edge carbon atoms. Similar to graphite, the Raman spectrum of SWCNTs shows as main lines the D-line at 1390 $cm^{-1}$, and the $G^+$-line 1594 $cm^{-1}$, slightly shifted when comparing with graphite, and an additional Raman band, the radial breathing mode (RBM) at 290 $cm^{-1}$, which can be used to calculate the diameter of the tubes. The ratio of D to $G^+$-line can be used advantageously in scans of SWCNTs to detect defects in the otherwise perfect periodically arranged atoms of the tube.[13] For the conventional Raman spectroscopy setup, a large quantity of SWCNTs are analysed at the same time and the average amount and type of defects can

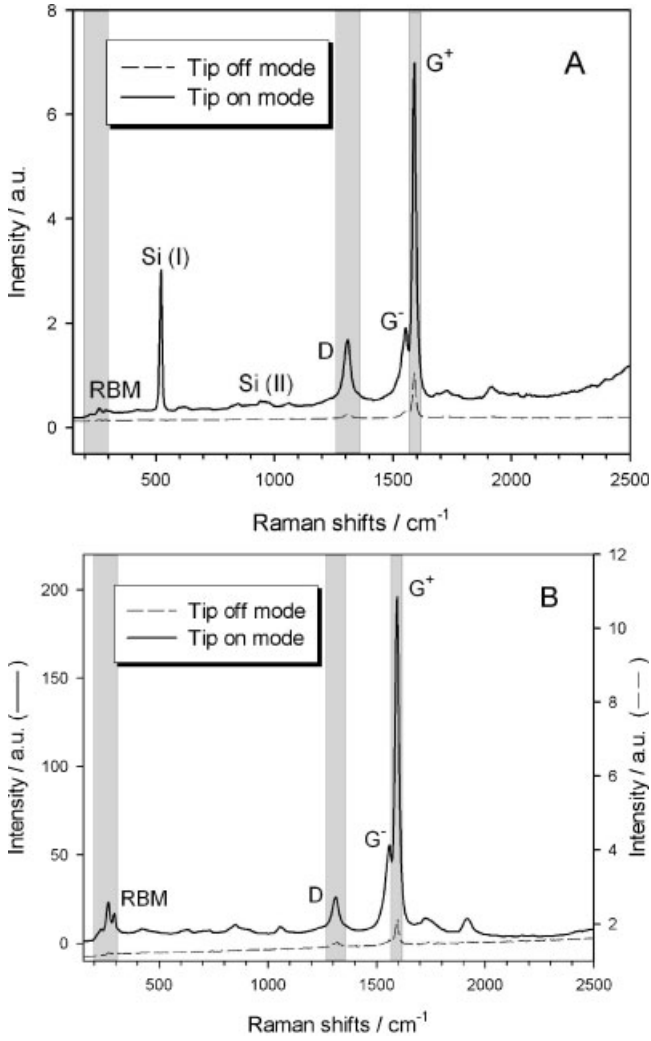


***Figure 6.***

Tip-enhanced Raman spectra of carbon nanotube bundles, (top) taken with a gold-coated AFM tip and (bottom) a self-made gold SFM tip. Note the much larger enhancement of the gold SFM tip (from Ref. 14).

 

be calculated, however, e.g. to learn more about local defect distribution at individual SWCNT to optimise procedures for functionalisation of SWCNTs, recently TERS was introduced.

Based on the concept of evanescent waves existing in the near-field (<100 nm) optical measurements beyond the diffraction limit are possible for attaining ultra-high resolution in optical spectroscopy. A practical implementation of that has become possible by combining optical spectroscopy and scanning probe microscopy (SPM), often referred to as apertureless near-field optical microscopy, and in particular, TERS. The crucial role in TERS is played by the SPM tip as a nanoscopic scatterer and/or lighting source. In the first case, the tip disturbs a confined non-radiating electromagnetic field in the proximity of a nanometer-sized specimen and converts it to a radiating one, which can be then detected by standard diffraction-limited optics. In the second case, a tip localises and enhances the scattered optical radiation over the incident one due to the coupled excitation of free electrons and the electromagnetic field present (called localised surface plasmon) in the metal of the tip. The latter is caused by the fact that namely metals, due to their small skin effect, provide the highest enhancement and scattering efficiency. An additional contribution to the field enhancement,

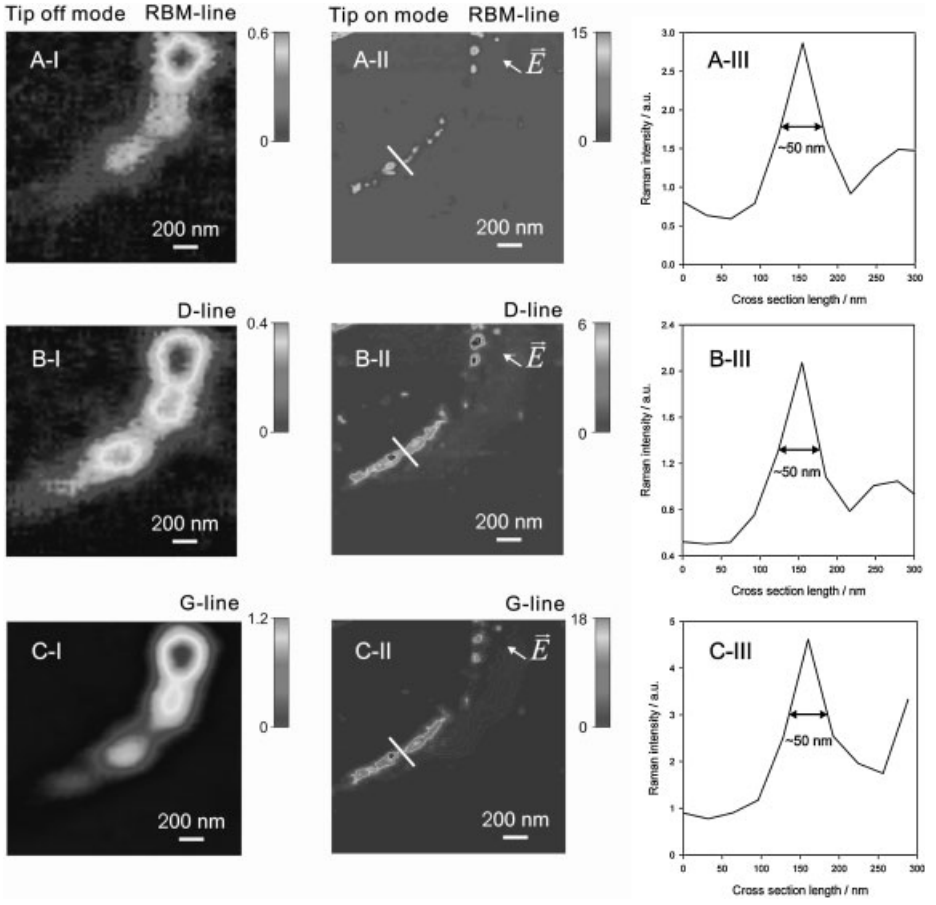


***Figure 7.***
Confocal (left) and tip-enhanced Raman (middle) scans on carbon nanotubes, using the radial breathing mode (RBM) line as well as the D- and $G^+$-lines. The cross sections indicated as a white bar in the middle scans are shown on the right (from Ref. 14).

 

known as quasi-static lighting rod effect, comes from a purely geometrical factor of the tip resulting in a quasi-singularity of the electromagnetic field near its apex. The material composition of the tip, its geometry and the polarization state of the incident light in the local excitation-based scheme are of the greatest importance for efficient enhancements.

Figure 6 shows tip-enhanced Raman spectra of SWCNT bundles that were taken with a gold-coated AFM tip as with a self-made gold SFM tip for tip-off (SPM tip is far away from the sample surface) and tip-on operation mode (tip is close to the sample surface and active in the nearfield). The gold SFM tip shows a much larger enhancement than the gold-coated AFM tip (256 compared to 9 for the G-line, linear enhancement, not area corrected). More details on the experiments performed can be found in reference.[14]

As the next step towards achievement of local Raman data by TERS is spectroscopic imaging. We have compared confocal and tip-enhanced Raman topographical scans on SWCNTs (Figure 7), using the radial-breathing mode (RBM) line as well as the D- and $G^+$-lines. Cross sections from these scans indicate a resolution of at least 50 nm (original data, 30 nm from a Gaussian fit) for the TERS scan, compared to approximately 300 nm for the confocal scan. These results demonstrate the potential of TERS imaging for local nanometer scale spectroscopic analysis of functional materials.

## Graphene

Finally, we would like to introduce first TERS data obtained on graphene. It has

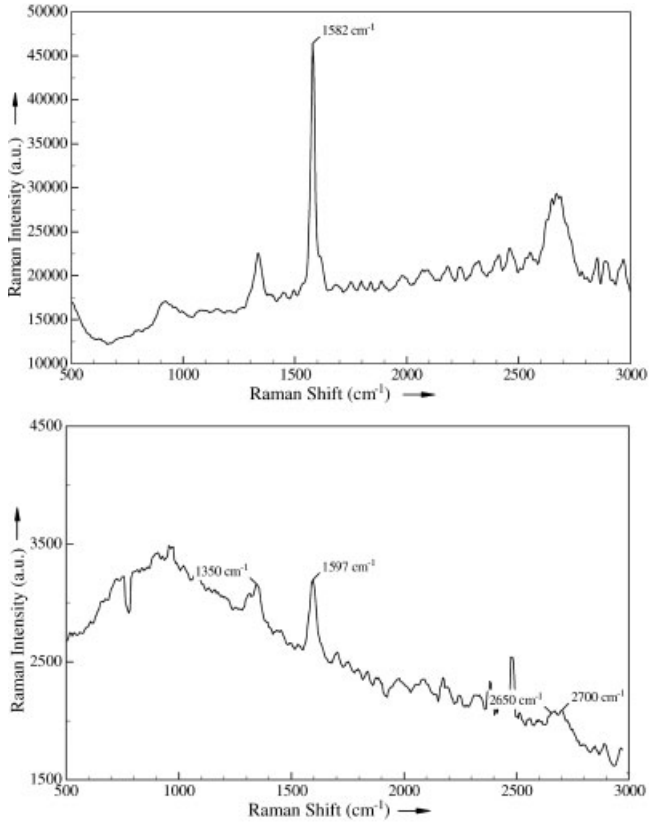


***Figure 8.***
Micro-Raman spectrum of (top) impure bulk grapheme, and (bottom) tip-enhanced Raman spectrum of impure graphene sheets.

 

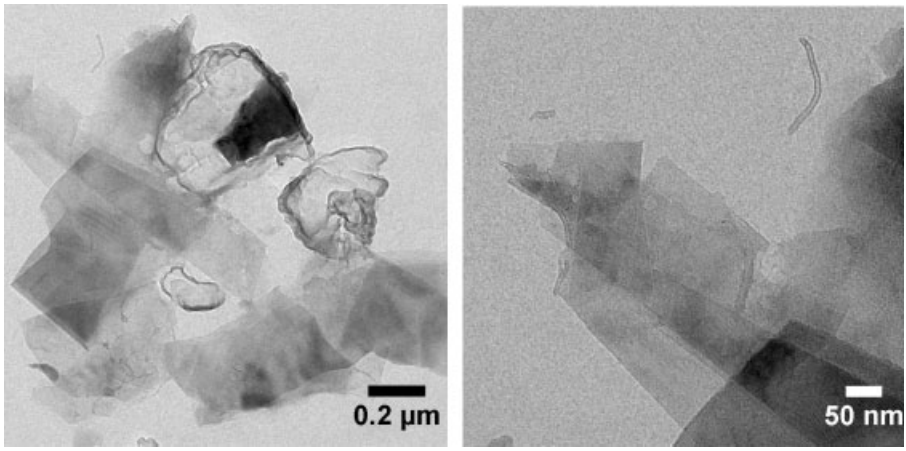


***Figure 9.***
TEM images of representative graphene samples.

been first described by Novoselov *et al.*[3] as monocrystalline graphitic films, which are a few atoms thick but are nonetheless stable under ambient conditions, metallic, and of remarkably high quality. The films were found by the authors to be a two-dimensional semimetal with a tiny overlap between valence and conductance bands. The conventional Raman spectrum of graphene and graphene layers has been studied in great detail by Ferrari *et al.*[21]. Graphene shows a Raman spectrum very similar to that of graphite, the differences observed mirror the missing interaction between the layers. The D peak second order changes in shape, width, and position for an increasing number of layers, reflecting the change in the electron bands via a double resonant Raman process, and the G peak slightly down-shifts.

We report here the first measured TERS spectrum of graphene. The graphene used by us has been prepared from HOPG and is still containing graphite flakes. These and the edges of the graphene flakes can be detected in the graphene bulk spectrum by the line at 1350 $cm^{-1}$ (Figure 8). A representative transmission electron microscopy (TEM) image of a similar sample is shown in Figure 9, which shows single as well as stacked layers of graphene. The spectrum was taken from a part of the sample (graphene and flakes) where no material was detected optically indicating only very little amount of material was present. The TERS spectrum suggests that the area under inspection was at the edge of graphene flakes, as the band at 2700 $cm^{-1}$ shows a split structure of approximately equal height, while pure graphene would only produce a single line (that at 2650 $cm^{-1}$). The band at 2700 $cm^{-1}$ in the graphite Raman spectrum at higher resolution has a shoulder at lower wavenumbers, it is the second order of zone-boundary phonons, the results presented are only preliminary data and our study of graphene still is in progress.

## Conclusion

Applying Raman spectroscopy helps understanding better the organisation of various carbon allotropes. Raman spectra of diamond, amorphous carbon, graphite, single wall carbon nanotubes (SWCNTs) and graphene sheets show different bands and band positions dependent on the degree of crystallinity, perfectness of their organisation or number of defects of the material under investigation. These variations can be used to determine the quality of the carbon-based materials, e.g. by comparing the intensities of the $G^{+}$- and D-bands. Ultimately, Raman spectroscopy combined with a scanning probe microscopy setup,

 

so-called apertureless near-field optical microscopy, and in particular tip-enhanced Raman spectroscopy and imaging, allows detection of such defects with lateral resolution in the nanometer range. We have demonstrated TERS on SWCNT and graphene samples, and in both cases high enhancement factors are obtained. In case of SWCNT, TERS imaging with lateral resolution far better than 50 nm is obtained and the results obtained reflect the local heterogeneity of individual SWCNTs on the nanometer length scale. Currently, similar investigations on graphene samples are in progress

*Acknowledgements:* The authors are grateful to Dr. J. Yu (Donghua University, Shanghai, China), Ing. S. van Bavel, and Dr. K. Lu for their help in preparing samples, to Dr. S. S Kharintsev and Dr. A. Kodentsov for carbon and graphite samples and stimulating discussions. The authors also acknowledge technical assistance from Dr. P. Dorozhkin and Dr. I. Dushkin (NT-MDT, Russia). This research has been supported by the Ministry of Economic Affairs of the Netherlands via the Technologische Samenwerkings project QUANAP (SenterNovem TSGE3108).

[1] H. Kroto, J. R. Heath, S. C. O'Brian, R. F. Curl, R. E. Smalley, *Nature* **1985**, *318*, 162.
[2] S. Iijima, *Nature* **1991**, *354*, 56.
[3] K. S. Novoselov, A. K. Geim, S. V. Morozov, D. Jiang, Y. Zhang, S. V. Dubonos, I. V. Grigorieva, A. A. Firsov, *Science* **2004**, *306*, 666.
[4] K. I. Katsnelson, *Materials today* **2007**, *10*, 20.
[5] J. Filik, *Spectroscopy Europe* **2005**, *17*, 10.
[6] I. R. Lewis, P. R. Griffith, *Appl. Spectrosc.* **1996**, *50*, 12A.
[7] R. K. Chang, "*Surface Enhanced Raman Scattering*", T. E. Furtak, Eds., Plenum Press, New York **1982**.
[8] Y. Inue, S. Kawata, *Opt. Lett.* **1994**, *19*, 159.
[9] L. Novotny, E. J. Sanchez, X. S. Xie, *Ultramicroscopy* **1998**, *71*, 21.
[10] E. J. Sanchez, L. Novotny, X. S. Xie, *Phys. Rev. Lett.* **1999**, *82*, 4014.
[11] A. Hartschuh, E. J. Sanchez, X. S. Xie XS, L. Novotny, *Phys. Rev. Lett.* **2003**, *90*, 095503.
[12] L. Novotny, S. J. Stranick, *Annu. Rev. Phys. Chem.* **2006**, *57*, 303.
[13] N. Anderson, A. Hartschuh, S. Cronin, L. Novotny, *J. Am. Chem. Soc.* **2005**, *127*, 2533.
[14] S. S. Kharintsev, G. G. Hoffmann, P. S. Dorozhkin, G. de With, J. Loos, *Nanotechnology* **2007**, *18*, 315502.
[15] D. S. Knight, W. B. White, *J. Mater. Res.* **1990**, *5*, 385.
[16] M. I. Nathan, J. E. Smith, Jr., K. N. Tu, *Journal of Applied Physics* **1974**, *45*, 2370.
[17] F. Tuinstra, J. L. Koenig, *J. Chem Phys.* **1970**, *53*, 1126.
[18] W. Krätschmer, K. Fostiropoulos, D. R. Huffman, *Chem. Phys. Lett.* **1990**, *170*, 167.
[19] D. S. Bethune, G. Meijer, W. C. Tang, H. J. Rosen, W. G. Golden, H. Seki, C. A. Brown, M. S. de Vries, *Chem. Phys. Lett.* **1991**, *179*, 181.
[20] J. Neugebauer, M. Reiher, C. Kind, B. A. Heß, *J. Comp. Chem.* **2002**, *23*, 895.
[21] A. C. Ferrari, J. C. Meyer, V. Scardaci, C. Casiraghi, M. Lazzeri, F. Mauri, S. Piscanec, D. Jiang, K. S. Novoselov, S. Roth, A. K. Geim, *Phys. Rev. Lett.* **2006**, *97*, 187401.

 